DAMAGE MECHANICS CHARACTERIZATION ON FATIGUE BEHAVIOR OF A SOLDER JOINT MATERIAL*

C. L. Chow and Fan Yang
Department of Mechanical Engineering
The University of Michigan-Dearborn
Dearborn, MI 48128

H. Eliot Fang
Computational Physics Department
Sandia National Laboratories
Albuquerque, NM 87185

ABSTRACT

This paper presents the first part of a comprehensive mechanics approach capable of predicting the integrity and reliability of solder joint material under fatigue loading without viscoplastic damage considerations. A separate report will be made to present a comprehensive damage model describing life prediction of the solder material under thermomechanical fatigue loading. The method is based on a theory of damage mechanics which makes possible a macroscopic description of the successive material deterioration caused by the presence of micro-cracks/voids in engineering materials. A damage mechanics model based on the thermodynamic theory of irreversible processes with internal state variables is proposed and used to provide a unified approach in characterizing the cyclic behavior of a typical solder material. With the introduction of a damage effect tensor, the constitutive equations are derived to enable the formulation of a fatigue damage dissipative potential function and a fatigue damage criterion. The fatigue evolution is subsequently developed based on the hypothesis that the overall damage is induced by the accumulation of fatigue and plastic damage. This damage mechanics approach offers a systematic and versatile means that is effective in modeling the entire process of material failure ranging from damage initiation and propagation leading eventually to macro-crack initiation and growth. As the model takes into account the load history effect and the interaction between plasticity damage and fatigue damage, with the aid of a modified general purpose finite element program, the method can readily be applied to estimate the fatigue life of solder joints under different loading conditions.

1. Introduction

The Pb-Sn eutectic alloy is widely used as a joining material in the electronics industry. In this application, the solder acts as both electrical and mechanical connections within and among the

* This work was supported by the United States Department of Energy under Contract DE-AC04-94AL85000. Sandia is a multiprogram laboratory operated by Sandia Corporation, a Lockheed Martin Company, for the United States Department of Energy.

DISCLAIMER

DISCLAIMER

Portions of this document may be illegible electronic image products. Images are produced from the best available original document.

different packaging levels in an electronic device. Advances in packaging technologies driven by the desire for miniaturization and increased circuit speed result in severe operating conditions for the solder joint. Specially, the mismatched thermal expansion characteristics of the materials joined by the solder and the cyclic temperature fluctuations normally encountered during service constitute a condition of thermomechanical fatigue (TMF) loading for the constrained solder joints. Therefore, the reliability and failure analysis of solder interconnections under fatigue loading becomes an important design issue as new electronic packaging technologies evolve.

A great deal of metallurgical information exists in the literature describing the response of solder alloys to conditions of thermomechanical loading with a variety of testing techniques [1]. However, the research on systematically interpreting and documenting solder fatigue behaviors is fairly recent. Given the microstructural complexity of solder behavior, the majority of the current methodologies are based on empirical curve fitting techniques, like the Coffin-Manson equation [2,3] in which a measurable physical quantity, usually the plastic strain range, is used as the basis for life prediction. The particular damage mechanisms associated with this physical quantity are usually not known. As this method at one time represented a major breakthrough in the field of low cycle fatigue, it is therefore not surprising that this semi-empirical method is frequently reported in the solder fatigue literature. Generally, TMF involves a combination of creep and plastic strains, and each can have a different effect on the component life. The Coffin-Manson equation does not allow differentiation between these two strains, resulting in difficulty in accurate life prediction. Another method, strain range partitioning (SRP) [4,5] more directly recognizes the separation and the combination of creep damage and fatigue damage processes in terms of the corresponding creep and plastic strains occurring in the stabilized cycle. These methods appear as interpolation rules more than general constitutive equations. They relate some stabilized cyclic conditions to the ultimate state of damage and ignore the progressive growth of the physical damage between the undamaged state and macroscopic crack initiation.

Another widely used approach involves the assessment of the fatigue life of solder material containing cracks based on the linear elastic fracture mechanics. The cyclic stress intensity factor ΔK and the cyclic J-integral range ΔJ have been widely recognized as being useful fracture mechanics parameters for analyzing crack growth. These parameters may be estimated by the finite element method when the structural and crack geometries are complex. The fatigue crack growth may thus be simulated by the relation between the crack growth rate and the parameter K or J. Strictly speaking, the equation $da/dN=f(K)$ or $da/dN=f(J)$ can only be employed to correlate test data under uniaxial tension-tension fatigue loading. The fracture mechanics approach should not therefore be indiscriminately translated into the fatigue design analysis of solder joints which are often three-dimensional in nature under non-proportional loading. Furthermore, when the crack length is physically short, the applicability of fracture mechanics becomes questionable. Experiments on the growth of short cracks have clearly shown that growth rates of short cracks are higher than those predicted by the conventional theory of fracture mechanics.

Another concern is that the traditional theory often assumes a material to be a flawless continuum at the micro-scale level. It is, however, well accepted that most engineering components contain both numerous micro-cracks and micro-voids developed during their manufacturing process and/or service loading. Consequently, the local response can be very different from macroscopic ones calculated or measured by most of the existing methods. In reality, the nucleation of a fatigue crack is a microscopic phenomenon within one or a few grains. That is why a direct approach through correlation of macroscopic test parameters, which is the basis of most conventional models, is questionable.

Because of the shortcomings and the limitations of the conventional fatigue damage analyses, a local approach known as the theory of damage mechanics has been employed to predict the fatigue behavior of cracks. The damage mechanics theory introduces a set of macroscopic internal state variables to describe the evolution of inherent micro-cracks and voids in the form of material degradation or damage. Fatigue damage is a form of material degradation caused by the initiation, growth and coalescence of micro-cracks in a material element due to cyclic loading and is therefore ideally suited to be characterized by the theory of damage mechanics. Nevertheless, only a few papers [7-22] have so far dealt with material damage behaviors subjected to fatigue loading.

Ideally, new analysis models should adequately represent material behavior on one hand but should, on the other hand, be sufficiently simple so that they are formulated in a form suitable for computational analysis. This paper describes the formulation of a method of fatigue residual life prediction based on a recently developed damage mechanics model [23-38]. Because of its inherent local approach, the unified failure criterion based on a critical material overall damage, which is considered an intrinsic material property and can be readily determined experimentally, has been proved to be valid in the characterization of not only damage evolution in an unnotched component but also crack initiation and propagation in a cracked one. With the introduction of a set of internal state variables, known as damage variables, and a damage effect tensor, damage dissipative potential functions are proposed to enable the formulation of the constitutive equations and a fatigue damage criterion. The fatigue evolution equation is subsequently formulated based on the hypothesis that the overall damage is induced by the accumulation of fatigue and plastic damages. The fatigue damage model is applied to estimate the fatigue life of 60Sn-40Pb solder material. An experimental analysis is also developed and used to successfully determine the mechanical properties of this material and its damage variables. The measured properties are presented and various damage characteristics of the solder material are examined and discussed.

2. Damage Mechanics Modeling

It is well accepted that microstructure of a solder joint cannot be ignored if its mechanical properties are to be fully understood. Changes in the microstructure can and do cause dramatic variations in mechanical properties and failure modes. However, it is extremely difficult for the current state of material science to provide the level of theoretical guidance that is needed to develop a predictive model based solely on micro-mechanics considerations. The current analysis is therefore intended to develop a hybrid micro-macro damage approach. Damage is herein defined as the gradual degradation or deterioration due to the presence of micro-voids/cracks in a solder material element under continuous load applications. A measure of the material degradation may be quantified at macro-scale level with an internal state variable known as damage variable **D**. The solder damage accumulation under fatigue loading may be sub-divided into two processes: plastic damage and fatigue damage. When the overall damage in a solder material element reaches a critical value, the element is said to be fully damaged resulting in final rupture.

2.1 Plasticity Damage

For the plasticity damage, the relationship between effective stress and strain tensors and their respective Cauchy stress and strain tensors may be expressed as [23]

$$\tilde{\mathbf{S}} = \mathbf{M}(\mathbf{D}):\mathbf{S} \tag{1}$$

$$\tilde{\mathbf{E}}^{e} = [\mathbf{M}(\mathbf{D})^{-1}]^{T} : \mathbf{E}^{e} \tag{2}$$

where $\mathbf{S}$ is the Cauchy stress tensor, $\tilde{\mathbf{S}}$ the effective stress tensor, $\mathbf{E}^e$ the elastic strain tensor, $\tilde{\mathbf{E}}^e$ the effective elastic strain tensor, and $\mathbf{M(D)}$ the damage effect tensor of fourth order.

Based on the concept of strain energy equivalence of Chow and Lu [36], the elastic energy for a damaged material is the same as that of the undamaged material, when the stress and strain tensors are replaced by the corresponding effective parameters in the stress/strain based form. It may be expressed in the stress-based form as

$$W^e(\mathbf{S},\mathbf{D}) = \frac{1}{2}\tilde{\mathbf{S}}:\mathbf{C}^{-1}:\tilde{\mathbf{S}} = \frac{1}{2}\mathbf{S}:\tilde{\mathbf{C}}^{-1}:\mathbf{S}, \quad \text{and} \quad \tilde{\mathbf{C}} = \mathbf{M(D)}^{-1}:\mathbf{C}:[\mathbf{M(D)}^{-1}]^T \tag{3}$$

where $W^e(\mathbf{S},\mathbf{D})$ is the elastic complementary energy and $\mathbf{C}$ represents the fourth-order elastic compliance tensor of the virgin material. The constitutive equation of elasticity is derived from thermodynamic theory in terms of true stress and strain expressed as

$$\mathbf{E}^e = \frac{\partial W^e(\mathbf{S},\mathbf{D})}{\partial \mathbf{S}} = \mathbf{C}^{-1}:\mathbf{S} \tag{4}$$

In the principal system of damage, the non-zero components in the matrix form of the damage effect tensor $\mathbf{M(D)}$ are expressed as

$$[M_{ij}(D)] = \begin{bmatrix} \frac{1}{1-D_1} & 0 & 0 & 0 & 0 & 0 \\ 0 & \frac{1}{1-D_2} & 0 & 0 & 0 & 0 \\ 0 & 0 & \frac{1}{1-D_3} & 0 & 0 & 0 \\ 0 & 0 & 0 & \frac{1}{1-\frac{1}{2}(D_2+D_3)} & 0 & 0 \\ 0 & 0 & 0 & 0 & \frac{1}{1-\frac{1}{2}(D_1+D_3)} & 0 \\ 0 & 0 & 0 & 0 & 0 & \frac{1}{1-\frac{1}{2}(D_1+D_2)} \end{bmatrix} \tag{5}$$

where D_1, D_2 and D_3 are the principal values of damage $\mathbf{D}$, which is a symmetric tensor of second order.

The evolution equations of plastic damage may be derived from the plastic damage energy release rate $\mathbf{Y_p}$, defined as

$$\mathbf{Y}_p = -\frac{\partial W^e(\mathbf{S},\mathbf{D})}{\partial \mathbf{D}} = -\mathbf{S}:(\tilde{\mathbf{C}}^{-1}:\mathbf{M}^{-1}:\frac{\partial \mathbf{M}}{\partial \mathbf{D}})^s:\mathbf{S} \tag{6}$$

in which the superscript "*s*" means that only the symmetric part should be taken. The plastic damage criterion F_{pd} is assumed as

$$F_{pd} = Y_{peq}^{1/2} - [C_{p0} + C_p(Z)] = 0 \tag{7}$$

where C_{p0} is the initial strengthening threshold, $C_p(Z)$ the increment of the threshold, Z the equivalent overall damage, and Y_{peq} is defined as

$$Y_{peq} = \frac{1}{2}\mathbf{Y_p}:\mathbf{L_p}:\mathbf{Y_p} \tag{8}$$

$\mathbf{L_p}$ is the fourth-order characteristic tensor of plastic damage and its matrix form may be expressed as

$$[L_{pij}] = \begin{bmatrix} 1 & \eta_p & \eta_p & 0 & 0 & 0 \\ \eta_p & 1 & \eta_p & 0 & 0 & 0 \\ \eta_p & \eta_p & 1 & 0 & 0 & 0 \\ 0 & 0 & 0 & 2(1-\eta_p) & 0 & 0 \\ 0 & 0 & 0 & 0 & 2(1-\eta_p) & 0 \\ 0 & 0 & 0 & 0 & 0 & 2(1-\eta_p) \end{bmatrix} \tag{9}$$

where η_p is assumed to be a material constant defining the degree of damage anisotropy.

If the plastic damage criterion of Eq. 7 is taken as the potential function, the plastic damage evolution equations become

$$\dot{Z}_p = \lambda_{pd} \frac{\partial F_{pd}}{\partial(-C_p)} = \lambda_{pd} \tag{10a}$$

and

$$\dot{\mathbf{D}}_\mathbf{p} = \lambda_{pd} \frac{\partial F_{pd}}{\partial(-\mathbf{Y_p})} = \frac{-\lambda_{pd}}{2Y_{peq}^{1/2}} \mathbf{L_p} : \mathbf{Y_p} \tag{10b}$$

where Z_p is the equivalent plastic damage and $\mathbf{D_p}$ is the plastic damage tensor. The Lagrange multiplier λ_{pd} can be evaluated, based on Eq. 7, as

$$\lambda_{pd} = \frac{\frac{\partial F_{pd}}{\partial \mathbf{S}} : \dot{\mathbf{S}} + \frac{\partial F_{pd}}{\partial \mathbf{D}} : \dot{\mathbf{D}}}{\left(\frac{\partial F_{pd}}{\partial C_p}\right)^2 \frac{\partial C_p}{\partial Z}} > 0, \text{ if } F_{pd} = 0 \text{ and } \frac{\partial F_{pd}}{\partial \mathbf{S}} : \dot{\mathbf{S}} + \frac{\partial F_{pd}}{\partial \mathbf{D}} : \dot{\mathbf{D}} > 0 \tag{11a}$$

or

$$\lambda_{pd} = 0, \text{ if } (F_{pd} < 0) \text{ or } (F_{pd} = 0 \text{ and } \frac{\partial F_{pd}}{\partial \mathbf{S}} : \dot{\mathbf{S}} + \frac{\partial F_{pd}}{\partial \mathbf{D}} : \dot{\mathbf{D}} \le 0 \tag{11b}$$

When the yield criterion of a material with damage F_p is defined as

$$F_p(\mathbf{S}, \mathbf{D}, R) = F_p(\tilde{\mathbf{S}}) - [R_0 + R(p)] = 0 \tag{12}$$

where R_o and R are initial and increment strain hardening thresholds, respectively, the constitutive plastic equations incorporating material damage may be derived by taking Eq. 12 as the potential function. The plastic strain tensor, $\mathbf{E_p}$, and the equivalent plastic strain, p, are therefore determined by the following equations

$$\dot{\mathbf{E}}_\mathbf{p} = \lambda_p \frac{\partial F_p}{\partial(\mathbf{S})} \tag{13a}$$

and

$$\dot{p} = \lambda_p \frac{\partial F_p}{\partial(-R)} = \lambda_p \tag{13b}$$

in which λ_p is determined by

$$\lambda_p = \frac{\frac{\partial F_p}{\partial \mathbf{S}}:\dot{\mathbf{S}} + \frac{\partial F_p}{\partial \mathbf{D}}:\dot{\mathbf{D}}}{\left(\frac{\partial F_p}{\partial R}\right)^2 \frac{\partial R}{\partial p}} > 0, \text{ if } F_p = 0 \text{ and } \frac{\partial F_p}{\partial \mathbf{S}}:\dot{\mathbf{S}} + \frac{\partial F_p}{\partial \mathbf{D}}:\dot{\mathbf{D}} > 0 \tag{14a}$$

or

$$\lambda_p = 0, \text{ if } (F_p < 0) \text{ or } (F_p = 0 \text{ and } \frac{\partial F_p}{\partial \mathbf{S}}:\dot{\mathbf{S}} + \frac{\partial F_p}{\partial \mathbf{D}}:\dot{\mathbf{D}} \le 0) \tag{14b}$$

Accordingly, the generalized constitutive formulation of damage characterization for solder material under substantial irreversible deformation is established, as shown in Eq. 13. The characterization also takes into account the effects of load history and the interaction between damage and plasticity.

2.2 Fatigue Damage

The fatigue damage is a microscopic change of material behavior at the scale of one or a few grains. At this scale the material is neither homogeneous nor isotropic, and the damage remains localized. In general, this difficult but challenging practical problem of localized damage has not yet received a rigorous mathematical treatment. As fatigue cracks always appear along the persistent slip bands due to localized plasticity, it is accordingly necessary to take into account the effect of plastic damage on the evolution of fatigue damage.

It is well accepted that the elastic strain energy conventionally defined for static loading is unable to describe the fatigue damage without suitable modifications. Its evolution equations may be derived from the cyclic elastic complementary energy $W_c^e(\mathbf{S_c}, \mathbf{D})$ defined as:

$$W_c^e(\mathbf{S}_c, \mathbf{D}) = \frac{1}{2}\tilde{\mathbf{S}}_c:\mathbf{C}^{-1}:\tilde{\mathbf{S}}_c = \frac{1}{2}\mathbf{S}_c:\tilde{\mathbf{C}}^{-1}:\mathbf{S}_c \tag{15}$$

$\mathbf{S_c}$ is the effective cyclic stress range tensor expressed as:

$$\tilde{\mathbf{S}}_c = \mathbf{M(D)}:\mathbf{S}_c = \mathbf{M(D)}:(\mathbf{S} - \mathbf{S}_{me}) = \tilde{\mathbf{S}} - \tilde{\mathbf{S}}_{me} \tag{16}$$

where $\mathbf{S}$ is the stress tensor, $\mathbf{S_{me}}$ the mean stress tensor given by

$$\mathbf{S}_{me} = \frac{1}{2}(\mathbf{S}_{max} + \mathbf{S}_{min}) \tag{17}$$

where $\mathbf{S_{max}}$ and $\mathbf{S_{min}}$ are the maximum stress tensor and the minimum stress tensor respectively. For multi-axial stress state, the terms "Maximum" and "Minimum" become ambiguous, but they may be regarded as two reverse points of a particular cyclic load range.

Similar to Eq. 6, the damage energy release rate $\mathbf{Y_f}$ corresponding to the fatigue damage can be obtained from

$$\mathbf{Y}_f = -\frac{\partial W_c^e(\mathbf{S}_c, \mathbf{D})}{\partial \mathbf{D}} = -\mathbf{S}_c:(\tilde{\mathbf{C}}^{-1}:\mathbf{M}^{-1}:\frac{\partial \mathbf{M}}{\partial \mathbf{D}})^s:\mathbf{S}_c \tag{18}$$

$\mathbf{Y_f}$ describes the variation of cyclic elastic strain energy due to cyclic loading, and is used to derive the evolution equations of fatigue damage.

During the nth cycle, the fatigue damage criterion is assumed as:

$$F_{fd} = Y_{feq}^{1/2} - [C_{f0}(\mathbf{S}_{me}) + C_f(Z_{fn}, Z)] = 0 \tag{19}$$

where C_{f0} $(\mathbf{S_{me}})$ is the initial strengthening threshold; $C_f(Z_{fn}, Z)$, the increment of the threshold; and Z_{fn}, the equivalent fatigue damage yielded at the nth cycle. Y_{feq} is defined as follows:

$$Y_{feq} = \frac{1}{2}\mathbf{Y_f} : \mathbf{L_f} : \mathbf{Y_f} \tag{20}$$

where $\mathbf{L_f}$ is the characteristic tensor of fatigue damage, which may be expressed as:

$$[L_{fij}] = \begin{bmatrix} 1 & \eta_f & \eta_f & & & \\ \eta_f & 1 & \eta_f & 0 & 0 & 0 \\ \eta_f & \eta_f & 1 & 0 & 0 & 0 \\ 0 & 0 & 0 & 2(1-\eta_f) & 0 & 0 \\ 0 & 0 & 0 & 0 & 2(1-\eta_f) & 0 \\ 0 & 0 & 0 & 0 & 0 & 2(1-\eta_f) \end{bmatrix} \tag{21}$$

where η_f is assumed to be a material constant.

If the fatigue damage criterion of Eq. 19 is taken as the energy dissipation function, the evolution equations of fatigue damage may be similarly derived as the plastic damage and expressed as:

$$\dot{Z}_{fn} = \lambda_{fd}\frac{\partial F_{fd}}{\partial(-C_f)} = \lambda_{fd} \tag{22}$$

$$\dot{\mathbf{D}}_{fn} = \lambda_{fd}\frac{\partial F_{fd}}{\partial(-\mathbf{Y_f})} = \frac{-\lambda_{fd}}{2Y_{feq}^{1/2}}\mathbf{L_f} : \mathbf{Y_f} \tag{23}$$

where the subscript "n" indicates the nth cycle.

The increments of fatigue damage and equivalent fatigue damage yielded in one cycle are

$$dZ = \frac{dZ_f}{dN} = dZ_f = \int dZ_{fn} \tag{24}$$

$$d\mathbf{D_f} = \frac{d\mathbf{D_f}}{dN} = \int d\mathbf{D}_{fn} \tag{25}$$

The integrals are conducted over one cycle. As the damage variable $\mathbf{D}$ is defined as the overall damage variable, including the fatigue damage and plastic damage, therefore,

$$d\mathbf{D} = d\mathbf{D_f} + d\mathbf{D_p} \tag{26}$$

where $\mathbf{D_f}$ and $\mathbf{D_p}$ are the fatigue damage and the plastic damage respectively.

3. Test Results and Model Validations

The proposed damage model calls for the determination of a number of damage variables which are considered as intrinsic material properties required as the finite element input data for predicting damage behaviors of solder joints. The solder material chosen for the investigation is the typical 60Sn-40Pb due to its prevalence in electronic applications. The material is assumed to be initially isotropic.

In order to demonstrate the validity of the proposed fatigue damage model, an investigation was first conducted to characterize damage behavior of the solder material under uniaxial tension and pure shear. Under uniaxial static loading, Eqs. 4, 7, and 10 may be reduced to

$$\tilde{E}_1 = E_1(1-D_1)^2, \quad \tilde{\nu}_{12} = \nu_{12}\frac{(1-D_1)}{(1-D_2)}, \quad Y_{peq}^{1/2} = \frac{\sigma_1^2}{\sqrt{2}E_1(1-D_1)^3} \tag{27a}$$

$$dD_1 = \frac{\sqrt{2}(1-D_1)\sigma_1 d\sigma_1}{2E_1(1-D_1)^4 \dfrac{\partial C_p}{\partial Z} - 3\sigma_1^2}, \quad D_2 = \eta_p D_1, \quad Z = \sqrt{2} D_1 , \tag{27b}$$

where $\tilde{E}_1$ and $\tilde{\nu}_{12}$ are the effective elastic modulus and Poisson's ratio, respectively.

A series of uniaxial tests for standard tensile specimens were conducted to measure the effective elastic modulus, the effective Poisson's ratio, and the true stress-strain curve. The measured mechanical properties of the material were in turn used to evaluate the plastic damage variables and their associated damage parameters based on the technique described in [23-25]. The specimen geometry depicted in Fig. 1 was chosen in accordance with the ASTM E8-93a standard. On the specimens, light machining grids l_o of 0.0394 inch division were made within the gauge length L_o of 2.9 inch for the purpose of plastic strain measurement. The experiments were conducted with an electro-hydraulic servo-controlled MTS 810 at room temperature. In determining the effective Young's modulus before necking, the total strains were measured using an extensometer (model MTS 632.12B-20). Upon unloading, the plastic strain was measured by recording the spacing between grid marks using a direct measuring microscope of 20 magnification with 0.0025 inch divisions. In evaluating the effective Young's modulus after necking, the strain upon reloading was measured with a strain gauge indicator (model P-3500) from strain gauges (type: FCA-2-11 rosette, resistance: 120.0±0.5Ω, gauge factor: 2.12±1.0%, manufactured by TML Tokyo Sokki Kenkyuju Co., Ltd.). The strain gauges and strain indicator were also used to measure the transverse strain under uniaxial tension to obtain initial and effective Poisson's ratios.

The deformation behavior of the specimen consists of three distinct phases, namely, uniform deformation, localized necking, and final rupture. At the initial loading when deformation was uniform, only spacing L_i between the first line and the last line, i.e., the current gauge length, needed to be measured, and the true strain was evaluated using

$$\varepsilon = \ln(L_i / L_o)$$

However, when localized plastic deformation in the necking area had occurred, spacing between two neighboring marks l_i was measured within the necking zone, and the true strain was calculated with

$$\varepsilon = \ln(l_i / l_o)$$

The variations of specimen width and thickness were also recorded to obtain the true stress as

$$\sigma = P_{app}/A$$

where P_{app} is the applied load and A, the current cross-section area.

For the sake of illustration, only the measured true stress-strain relationship at the rate of 0.25 inch/min is shown in Fig. 2. The measurement of the effective Young's modulus and Poisson's ratio enables the determination of the damage variable D_1 and D_2 from Eq. 27a. Evolution of damage variables D_1 and D_2 against strain at the rate of 0.25 inch/min are shown in Fig. 3, indicating some degree of plastic damage anisotropy at higher strain. This confirms the need to incorporate the proposed damage coefficient of $\mathbf{L_p}$ for an accurate approximation to the actual damage progression. These curves were then used to deduce the value of parameter η_p to be 0.834. The increment of plastic damage threshold C(Z) can also be readily evaluated experimentally as a function of the equivalent plastic damage as shown in Fig. 4.

Since solder joints often fail in shear, a validation analysis was next performed to simulate pure shear failure. The geometry of the specimen shown in Fig. 5 was prepared in accordance

with the ASTM B831-93 standard for pure shear test. To predict the ultimate shear strength of the material analytically, the plastic damage parameters determined under the uniaxial load were used as input data. The slope $\partial C_p/\partial Z$, required in Eq. 27b, was obtained from the curve depicted in Fig. 4. The critical value of equivalent overall damage Z_{cr}, which had been used to determine the material final failure, was found to be 0.53 according to the value of D_1 shown in Fig. 3 and the expression of Z given in Eq. 27b. From Eqs. 9 and 10, the predicted shear ultimate strength for the specimen shown in Fig. 5 is 3.12 ksi, which compares satisfactorily with the experimental value of 2.84 ksi, producing a discrepancy of 10%. The result of shear stress analysis confirms the validity, accuracy and applicability of the damage model for pure shear, which is considered to be the predominant mode of failure experienced in solder joints.

Another investigation was conducted to examine the validity of the proposed fatigue damage model for the prediction of fatigue life of unnotched specimens under varying stress amplitudes. The validation analysis requires for the first instance the determination of fatigue damage variables and parameters shown in Eq. 28. The configuration of fatigue test specimen shown in Fig. 6 is chosen in accordance with the ASTM standard described in STP 566. The experiments were carried out under load-control at room temperature and the frequency of the tests was 5Hz.

The incremental fatigue damage is a localized phenomenon and is therefore impractical to be measured each cycle. The increment of strengthening threshold of fatigue damage $C_f(Z_{fn}, Z)$ in Eq. 19 may be expressed as:

$$C_f(Z_{fN}, Z) = Z_{fN} C_{f1} Z^{C_{f2}} \tag{28}$$

Under uniaxial cyclic stress, $\sigma_1 \neq 0$, $\sigma_2 = \sigma_3 = 0$, Eqs. 24 and 25 become

$$Z_{fN} = \frac{dZ_f}{dN} = \int_{\sigma_{ct1}}^{\sigma_{c\max 1}} \frac{\sqrt{2}\sigma_{c1} d\sigma_{c1}}{E(1-D_1)^3 \dfrac{\partial C_f}{\partial Z_{fN}}} = \frac{(\sigma_{c\max 1} - \sigma_{me1})^2 - \sigma_{ct1}^2}{\sqrt{2}E(1-D_1)^3 \dfrac{\partial C_f}{\partial Z_{fN}}} \tag{29}$$

$$D_{fN1} = \frac{dD_{f1}}{dN} = \int_{\sigma_{ct1}}^{\sigma_{c\max 1}} \frac{\sigma_{c1} d\sigma_{c1}}{E(1-D_1)^3 \dfrac{\partial C_f}{\partial Z_{fN}}} = \frac{(\sigma_{c\max 1} - \sigma_{me1})^2 - \sigma_{ct1}^2}{2E(1-D_1)^3 \dfrac{\partial C_f}{\partial Z_{fN}}} \tag{30}$$

σ_{max1} is the maximum stress in a cycle, σ_{me1} is the mean stress, and σ_{ct1} is the threshold value of σ_{c1} which takes into account the effect of mean stress by means of Goodman's formula [39].

With Eq. 28, integrating Eq. 29 over N cycles with respect to the equivalent overall damage Z, the number of fatigue cycles can be obtained,

$$\begin{aligned} N &= \frac{\sqrt{2}E}{(\sigma_{max1} - \sigma_{me1})^2 - \sigma_{ct1}^2} \int_{Z_o}^{Z} \left(1 - \frac{Z}{\sqrt{2}}\right)^3 C_{f1} Z^{C_{f2}} dZ \\ &= \frac{\sqrt{2}EC_{f1}}{(\sigma_{max1} - \sigma_{me1})^2 - \sigma_{ct1}^2} [G_f(Z) - G_f(Z_0)] \end{aligned} \tag{31}$$

where

$$G_f(Z) = \frac{Z^{C_{f2}+1}}{C_{f2}+1} - \frac{3Z^{C_{f2}+2}}{\sqrt{2}(C_{f2}+2)} + \frac{3Z^{C_{f2}+3}}{2(C_{f2}+3)} - \frac{Z^{C_{f2}+4}}{2\sqrt{2}(C_{f2}+4)}$$

and Z_o is the initial overall damage.

The parameters of plastic damage determined by the procedure described above are used as initial input data for fatigue analysis. In order to determine the fatigue damage parameters C_{f1}

and C_{f2}, several groups of uniaxial fatigue test under the single block symmetric loading are conducted. The range of maximum stress is varied from 2.3 ksi to 5.1 ksi.

If let

$$f(C_{f1}, C_{f2}) = \sum_{i=1}^{NN} [N^i_{cal}(C_{f1}, C_{f2}) - N^i_{exp}]^2$$

where NN is the group number of the test, N_{cal} and N_{exp} are calculated and experimental cycle numbers, respectively, C_{f1} and C_{f2} are evaluated by using the numerical scheme described in Fig. 7. The parameters obtained are: $C_{f1} = 825$ and $C_{f2} = -0.0291$. $C_{f2} < 0$ means that the development of fatigue damage is exponentially increased as a function of the overall equivalent damage Z. The endurance life chosen to define the endurance limit required by the damage model is 10^6 cycles which is considered reasonable as the fatigue life of the solder joint material is estimated between 10^3 and 10^5 cycles. The measured endurance limit σ_{c1} in Eq. 29 is 2.35 ksi. The element η_f in the characteristic tensor of fatigue damage $\mathbf{L_f}$ is assumed to be equal to η_p. The predicted results are shown in Table 1 and Fig. 8, where σ_{max} is the maximum stress; σ_{min}, the minimum stress; N_{exp}, the experimental fatigue life; N_{pre}, the predicted fatigue life calculated with Eq. 31. The prediction confirms the validity and accuracy of the fatigue damage parameters, C_{f1} and C_{f2}. These damage parameters will be employed for the fatigue analysis of solder joint structure.

σ_{max}	σ_{min} (ksi)	N_{exp} ($\times 10^3$)	N_{pre} ($\times 10^3$)
5.12	–5.12	29.36	25.11
4.49	–4.49	50.22	53.15
4.33	–4.33	56.03	60.24
3.53	–3.53	142.12	116.65

Table 1. Fatigue Life with Constant Amplitude Cycling

The proposed fatigue damage model is also applied to predict the fatigue life of solder specimen subjected to variable amplitude fatigue loading. Table 2 provides a comparison between the experimental and predicted results. Fig. 9 provides a graphical representation of the first two variable-amplitude cycle stresses summarized in Table 2.

initial σ_{max}	σ_{min} (ksi)	N_{exp} ($\times 10^3$)	N_{pre} ($\times 10^3$)
4.69	0.18	5.2	3.6
3.04	0.027	53.3	51.0
3.69	–2.55	133.66	151.52

Table 2. Fatigue Life with Variable Amplitude Cycling

4. CONCLUSIONS

A fatigue damage model, which takes into account the gradual material degradation or deterioration resulting from the initiation, growth and coalescence of micro-cracks/voids in a material element, has been developed for a solder joint material. The state variable theory coupled

with the monotonic elastic strain energy release rate $\mathbf{Y_p}$ and the cyclic elastic strain energy release rate $\mathbf{Y_f}$ is introduced to formulate the constitutive equations and plastic and fatigue damage evolution laws. Fatigue life prediction is realized from the summation of the accumulated plastic and fatigue damages. An extensive experimental program has been conducted to determine the damage parameters, which are used to evaluate the progressive material degradation in terms of effective Young's modulus and Poisson's ratio. As shear mode of fracture is often observed in solder joints, the damage analysis is then applied to predict shear fracture stress which compares favorably with the test results. The measured damage parameters have also been applied and found to yield a satisfactory prediction of the fatigue life of the solder joint material under variable-amplitude cycle loading conditions. These comparisons confirm the validity of the proposed damage model in characterizing damage behaviors of the solder joint material.

It is well recognized that solder joints in real life are subjected to a combination of thermal and mechanical cycling. The solder material also exhibits significant strain-rate dependency at operating temperatures. A program to extend the current damage mechanics model and characterization to include the effects of temperatures, strain rates, and creep damages in the Pb-Sn solder joint material is being actively pursued. The proposed damage model will also be implemented in a general purpose finite element package. The implementation aims at providing a comprehensive engineering tool for a real-life solder joint analysis and an acid test by comparing its predictions with experimental measurements in some simple yet practical solder joints. This will include damage behavior analysis of a 60Sn-40Pb solder joint connecting a typical chip carrier and a printed wiring board subjected to a spectrum of fatigue loads.

ACKNOWLEDGMENT

C. L. Chow and Fan Yang wish to gratefully acknowledge support of this research through a contract with Sandia National Laboratories.

References

[1] "The Mechanics of Solder Alloy Interconnects", Edited by D.R. Frear, S.N. Burchett, H.S. Morgan, & J.H. Lau, Van Nostrand Reinhold, New York, 1994.

[2] Coffin, L.F., "Fracture", Chapman and Hall, London, 1969.

[3] Masson, S.S., "Thermal Stress and Low-Cycle Fatigue", McGraw-Hall, New York, 1966.

[4] Masson, S.S., Halford, G.R., & Hirschberg, M.H., "Creep-Fatigue Analysis by Strain-Range Partitioning", NASA TMX 67838, Symposium on Design for Elevated Temperature Environment, ASME, 1971

[5] Hirschberg, M.H. and Halford, G.R., "Strain-Range Partitioning-A Tool for Characterizing High-Temperature Low-Cycle Fatigue", NASA TMX 71691, 1975.

[6] Solomon, H.D., "Life Prediction and Accelerated Testing", *The Mechanics of Solder Alloy Interconnects*, Edited by D.R. Frear, S.N. Burchett, H.S. Morgan, & J.H. Lau, Van Nostrand Reinhold, New York, 1994, pp199-313.

[7] Chaboche J.L., Kaczmarek, H. and Paine, J., "Hardening and fatigue damage interaction in 316 Al Steel", La Rech. Aerospatiale (English Edition), (1980), 35-55.

[8] Chaboche, J.L. and Lesne, P.M., "On the non linear fatigue damage accumulation", International Conference on Steel Structures, Budva (Yougoslavie), (1986).

[9] Chaudonneret, M. and Chaboche, J.L., "Fatigue life prediction of notched specimens", International Conference on Fatigue of Engineering Materials and Structures, University of Sheffield (U.K.), (1986).
[10] Beaumont, P.W.R., "The fatigue damage mechanics of composite laminates", Damage Mechanics in Composites edited by A.S.D. Wang and G. K. Haritos, AD-12 (1987), 53-63.
[11] Chaboche, J.L., "Continuum damage mechanics and its application to structural lifetime predictions", Rech. Aerosp., (1987), 37-54.
[12] Chaboche J.L. and Lesne, P.M., "A non-linear continuous fatigue damage model", Fatigue Fract. Engng Mater. Struct, 11 (1988), 1-17.
[13] Suresh S., "Mechanics and micromechanism of fatigue crack growth in brittle solids", International Journal of Fracture, 42 (1990), 41-56.
[14] Lemaitre, J., "Micro-mechanics of crack initiation", International Journal of Fracture, 42 (1990), 87-99.
[15] McEvily, A.J., "Current aspects of fatigue", Metal Science, August/September, (1977), 274-284.
[16] Fine, M.E., "Fatigue resistance of metals", Met. Trans. A, 11A (1980), 365-379.
[17] Gerold, V. and Meier, B., "Deformation mechanisms and crack initiation in fatigue", Fatigue 87 (Edited by R. O. Ritchie and E. A. Starke), EMAS, (1987), 1517-1540.
[18] Lu, T.J. and Chow, C.L., "On constitutive equations of inelastic solids with anisotropic damage", Theor. Appl. Frac. Mech., 14 (1990), 187-218.
[19] Chow, C.L. and Wei, Y., "A model of continuum damage mechanics for fatigue failure", Inter. J. Frac., 50 (1991), 301-316.
[20] Chow, C.L. and Wei, Y., "A damage mechanics model of fatigue crack initiation in notched plates", Theoretical and Applied Fracture Mechanics, 16 (1991), 123-133.
[21] Wei, Y., Chow, C.L., and Duggan, B.J., "A damage model of fatigue analysis for AL alloy 2024-T3", Advances in Engineering Plasticity and Its Application, Edited by W.B. Lee, Elsevier, (1993), 325-332
[22] Wei, Y., Chow, C.L., and Duggan, B.J., "Finite element analysis of fatigue crack growth with damage mechanics", Proceedings of the Joint ASCE-ASME-SES Meeting, June, 1993.
[23] Chow, C.L. and Wang, J., "An anisotropic theory of elasticity for continuum damage mechanics", International Journal of Fracture, 33 (1987), 3-16.
[24] Chow, C.L. and Wang, J., "An anisotropic theory of continuum damage mechanics for ductile fracture", Engineering Fracture Mechanics, 27 (1987), 547-558.
[25] Chow, C.L. and Wang, J., "An anisotropic continuum damage theory and its application to ductile crack initiation", Damage Mechanics in Composites, ASME, AD-12 (1987), 1-10.
[26] Chow, C.L. and Wang, J., "Mixed mode fracture criteria for ductile materials", Pressure Vessel Technology, Proc. ICPVT-6, Beijing, 2 (1988), 791-197.
[27] Chow, C.L. and Wang, J., "A finite element analysis of continuum damage mechanics for ductile fracture", International journal of fracture, 38(1988), 83-102.
[28] Chow, C.L. and Wang, J., "Ductile fracture Characterization with an anisotropic continuum damage theory", Engineering Fracture Mechanics, 30(1988), 547-563.
[29] Chow, C.L. and Wang, J., "On crack initiation angle of mixed mode ductile fracture with continuum damage mechanics", Engineering Fracture Mechanics, 32 (1989), 601-612.
[30] Wang, J. and Chow, C.L., "A non-proportional loading finite element analysis of continuum damage mechanics for ductile fracture", International Journal for Numerical Methods in Engineering, 29 (1990), 197-209.

[31] Wang, J. and Chow, C.L., "Subcritical crack growth in ductile fracture with continuum damage mechanics", Engineering Fracture Mechanics, 33 (1989), 309-317.
[32] Chow, C.L. and Wang, J., "Crack propagation in mixed mode ductile fracture with continuum damage mechanics", Mechanical Engineering Science, Proceeding of Institute of Mechanical Engineers, Part C, 203 (1989), 189-199.
[33] Wang, J. and Chow, C.L., "Mixed mode ductile fracture studies with non-proportional loading based on continuum damage mechanics", ASME Tran., Journal of Engineering Materials and Technology, 111 (1989), 204-209.
[34] Wang, J. and Chow, C.L., "Hysteretic effect of damage and stress on ductile fracture characterization", Engineering Fracture Mechanics, 34 (1989), 209-220.
[35] Chow, C.L. and Wang, J., "Mixed mode ductile fracture characterization with a continuum damage mechanics model", Proceeding of FEFG Workshop, Role of Plasticity and Damage Mechanics in Fracture of Solids, (1988), 93-99.
[36] Chow, C.L. and Lu, T.J., "On evolution laws of Anisotropic Damage", Engineering Fracture Mechanics, 34 (1989), 679-701.
[37] Chow, C.L. and Lu, T.J., "A normative representation of stress and strain for continuum damage mechanics", Theoretical and Applied Fracture Mechanics, 12 (1989), 161-187.
[38] Chow and K.Y. Sze, "Characterization of notched ductile failure with continuum damage mechanics", Journal of Engineering Materials and Technology, 112 (1990), 412-421.
[39] Goodman, J, "Mechanics Applied to Engineering", Longmans, Green & Co., Ltd., London, (1899).

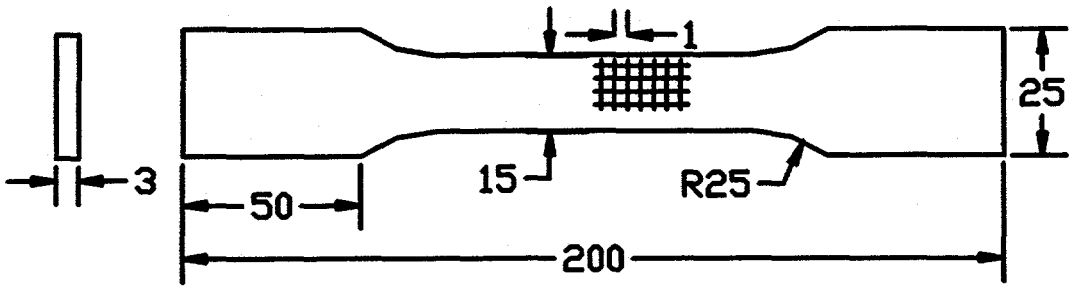

Fig.1 Tension test specimen(all unit: mm)

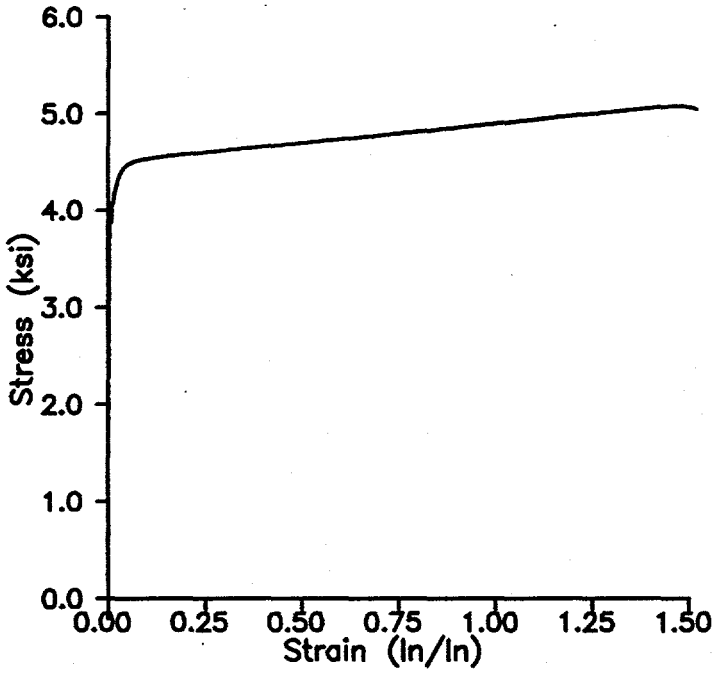

Fig.2 True stress-strain curve for 0.25 in/min

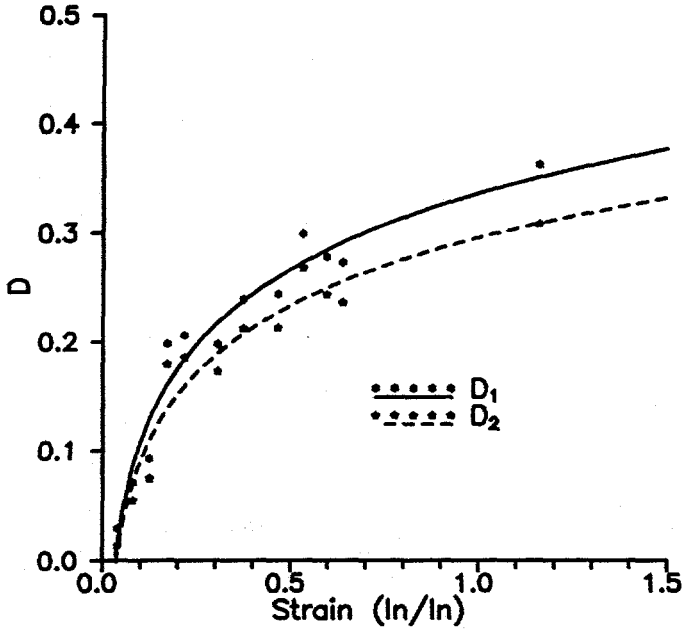

Fig.3 Evolution of damage with strain

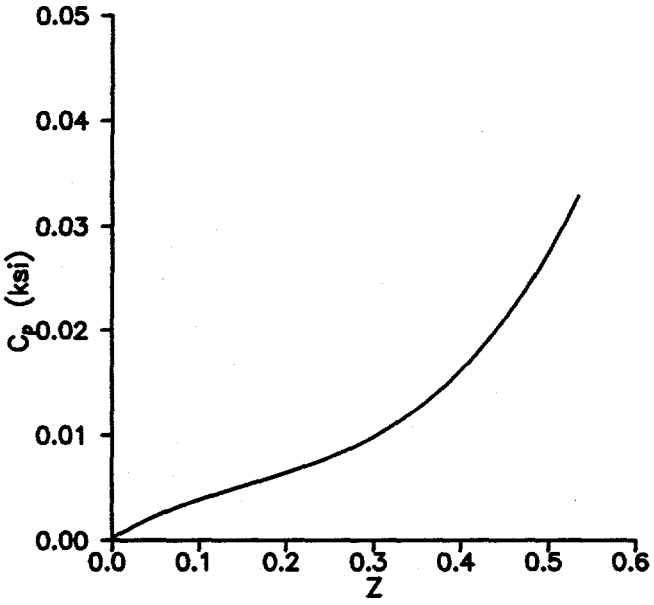

Fig.4 C_p-Z curve

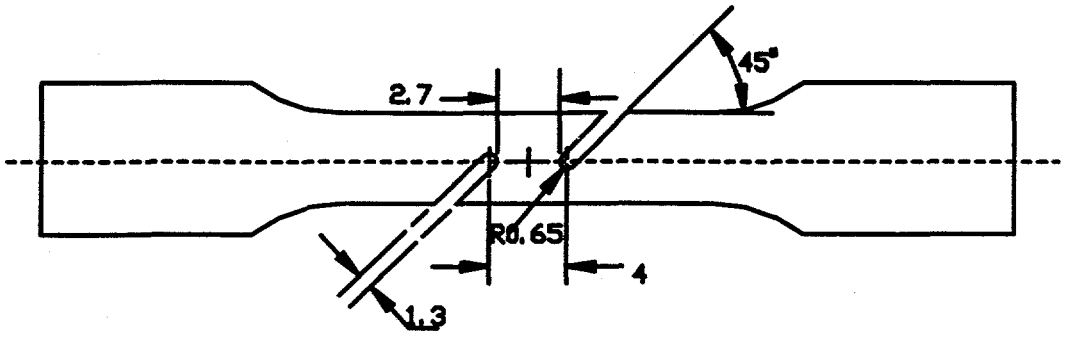

Fig.5 Shear test specimen (all unit: mm)

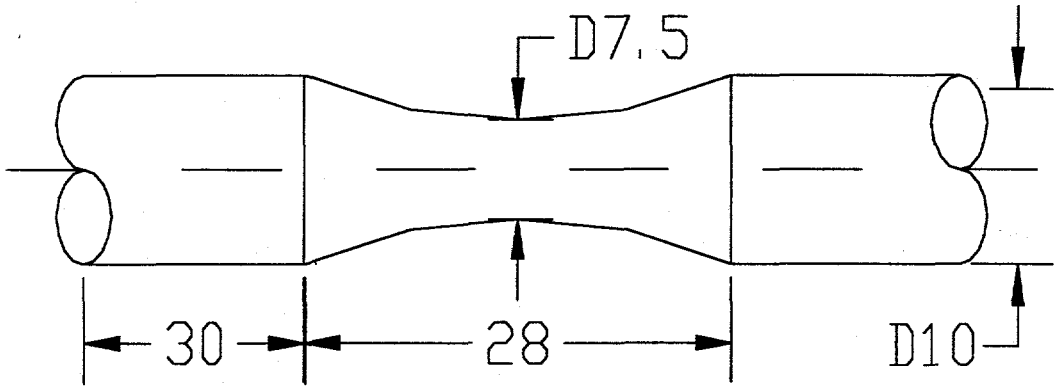

Fig.6 Fatigue specimen geometry

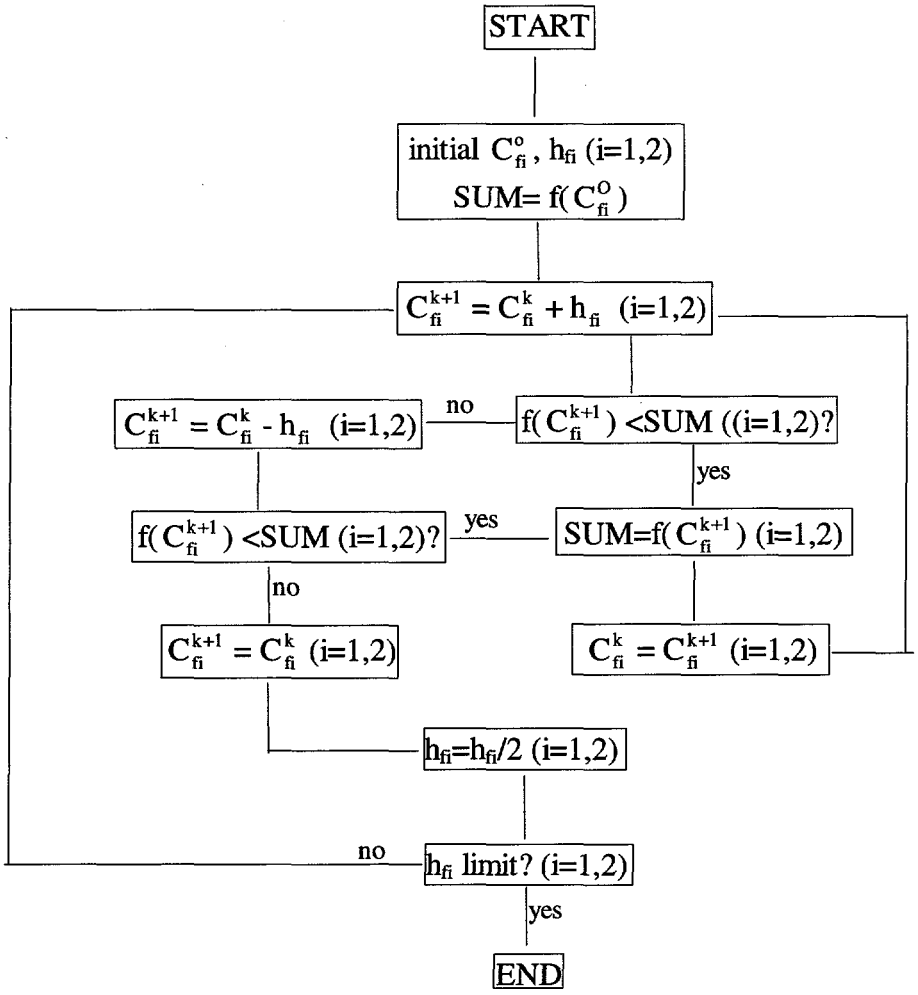

Fig. 7 Flow Chart of determining C_{f1} and C_{f2}

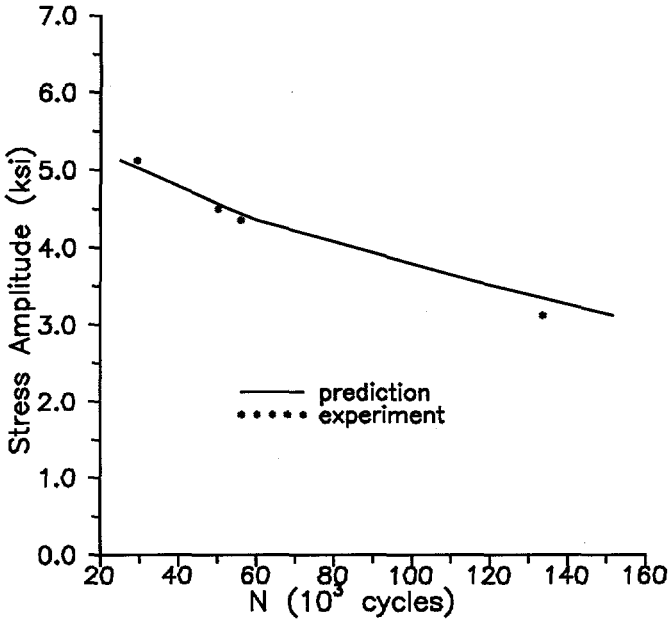

Fig.8 Fatigue Life with constant amplitude cycling

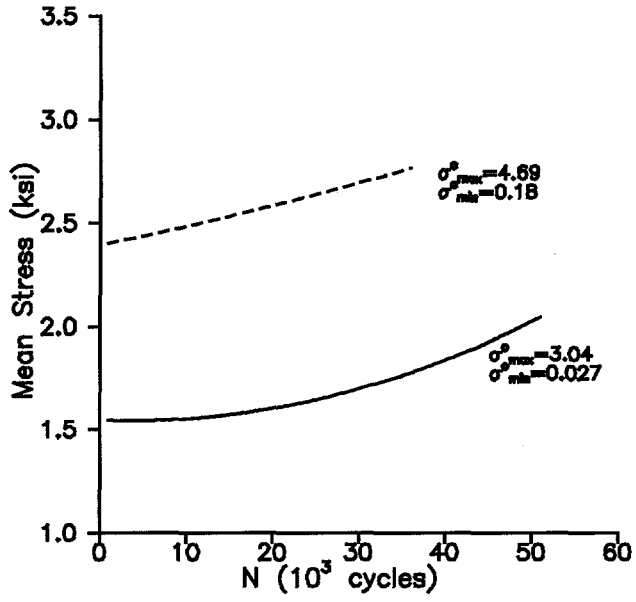

Fig.9 Variable-amplitude stress cycling